How to cite: *Angew. Chem. Int. Ed.* **2024**, *63*, e202313679
doi.org/10.1002/anie.202313679

Quantum Chemistry

Tipping the Balance Between the bcc and fcc Phase Within the Alkali and Coinage Metal Groups

Andrés Robles-Navarro, Paul Jerabek,* and Peter Schwerdtfeger**

Abstract: Why the Group 1 elements crystallize in the body-centered cubic (bcc) structure, and the iso-electronic Group 11 elements in the face-centered cubic (fcc) structure, remains a mystery. Here we show that a delicate interplay between many-body effects, vibrational contributions and dispersion interactions obtained from relativistic density functional theory offers an answer to this long-standing controversy. It also sheds light on the Periodic Table of Crystal Structures. A smooth diffusionless transition through cuboidal lattices gives a detailed insight into the bcc→fcc phase transition for the Groups 1 and 11 elements.

Chemical intuition using basic bonding models, such as the ball-and-stick model, the VSEPR (valence-shell electron repulsion) model, hybridization concepts, covalent and ionic models, ligand-field theory or force field methods, to name but a few, is extremely successful in predicting molecular structures and chemical reaction paths.[1,2] We cannot imagine chemistry anymore without the use of such qualitative bonding models. However, such simple bonding models do not necessarily transfer so easily into the solid state where one requires a more elaborate quantum theoretical treatment and sophisticated algorithms[3] to correctly predict crystal structures at certain temperatures and pressures. This conundrum between the gas phase and the solid state was nicely summarized by John Maddox in 1988: *One of the continuing scandals in the physical sciences is that it remains in general impossible to predict the structure of even the simplest crystalline solids from a knowledge of their chemical composition.*[4]

A statistical evaluation of low-temperature crystal structures for 102 elements in the Periodic Table shows that the majority crystallize either in the face-centered cubic (fcc) or hexagonal close-packed (hcp) phase (48 %), as one expects from a maximal packing density of $\rho_{fcc}=\rho_{hcp}=\pi\sqrt{18}$ (74.05 %) and a high coordination number of $N_{CN}=12$. Far fewer elements crystallize in the body-centered cubic (bcc) structure (21 %) having a much lower packing density of $\rho_{bcc}=\pi\sqrt{3/8}$ (68.02 %) and $N_{CN}=8$. As prime examples, the known Group 1 solids all adopt the bcc lattice, while in contrast the Group 11 elements adopt the fcc lattice at standard conditions.

We recently argued that the bcc phase for the lightest Group 1 element, lithium, is stabilized over the fcc structure by zero-point vibrational effects.[5] This vibrational stabilization of the bcc phase is further enhanced by temperature effects through the Boltzmann distribution and the vibrational entropy term, which gives an atomistic explanation of the Landau theory favouring the bcc phase close to the melting point.[6] However, lithium is quite different to the other Group 1 elements. Furthermore, zero-point vibrational effects are much smaller for the heavier Group 1 elements and one therefore seeks a different explanation for the dominance of the bcc phase within the (heavier) Group 1 metals. We therefore decided to carry out relativistic density functional calculations along the path of smooth cuboidal (body-centered tetragonal structures) transformations from bcc to fcc, see Figure 1. The important role of dispersion effects will be highlighted by using Grimme's add-on dispersionenergy correction, as well as relativistic effects for both silver and gold. We use the formalism as

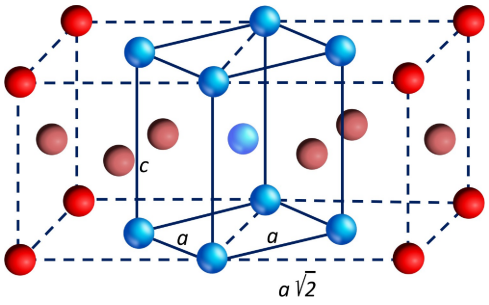

Figure 1. Body-centered tetragonal lattice shown in blue with lattice constants a and c. For $a=c$ we obtain the bcc lattice. The usual fcc unit cell with additional red atoms is shown as well with lattice constants $a'=a\sqrt{2}=c$.

[*] A. Robles-Navarro, Prof. Dr. P. Schwerdtfeger
Centre for Theoretical Chemistry and Physics, The New Zealand Institute for Advanced Study (NZIAS), Massey University Albany Private Bag 102904, Auckland 0745, New Zealand
E-mail: a.roblesnavarro@massey.ac.nz
peter.schwerdtfeger@gmail.com

Dr. P. Jerabek
Institute of Hydrogen Technology,
Helmholtz-Zentrum Hereon
Max-Planck-Str. 1, 21502 Geesthacht, Germany
E-mail: paul.jerabek@hereon.de

outlined by Jerabek et al.[5] which involves only a single cuboidal distortion parameter A with $A=1$ set for fcc and $A=1/2$ for bcc (see computational details).

Alkali metals are well-known for crystallizing into the bcc phase at standard conditions, however, some density functionals predict other phases like fcc or hcp to be more stable at 0 K as the energy differences between the different structures can be very small.[7,8] To analyse this in more detail, the cohesive energy with respect to the fcc phase along the cuboidal (Bain) distortion path[9] is obtained from density functional calculations (see computational details) for the alkali metals from Li to Fr as depicted in Figure 2. Care had been taken to converge the PBE calculations to the required accuracy of 10^{-3} kJ/mol. As can be seen, the differences in the cohesive energy between the bcc and fcc phases for each alkali metal are of the order of 0.1 kJ/mol (see Table 1), which provides a challenge to such calculations.[10] Nevertheless, when adding dispersion corrections by means of Grimme's DFT-D3(BJ) method,[11] the bcc phase of the Group 1 metals with the exception of lithium becomes stabilized with respect to fcc, but obviously not enough for francium to make bcc the most stable phase. This may however change with different density functional approximations, which is currently under investigation by our group. Thermal contributions to the free energy will further stabilize the bcc phase as already pointed out.[5]

Regarding the dispersion interaction we plot the ratio $q_{\mathrm{disp}}(A)=E_{\mathrm{disp}}(A)/E_{\mathrm{disp}}(1)$ in Figure 3 to point towards a very similar functional behavior for all the elements considered here. This ratio varies smoothly along the Bain path, having a maximum at the bcc phase. Further, the magnitude of the dispersion energy among the alkali metals is the highest in lithium. This is perhaps surprising as the dipole polarizabilities for the alkali atoms increase down the group (except for francium and element 119 where relativistic effects become important)[12] and the coordination number is 12 in fcc compared to only 8 in bcc. However, as defined in the DFT-D3(BJ) method,[11] the magnitude of the dispersion energy will critically depend on the nearest neighbor distance for all systems as the dominant London dispersion term is $\sim R^{-6}$. Further, the nearest neighbor distance decreases from fcc to bcc along the Bain path, see Table 1. Nonetheless, in Figure 4 we see an overall destabilization of the bcc phase for lithium compared to its fcc phase. Although dispersion interactions are always stabilizing, we notice that the electronic energy in the dispersion-corrected crystal is higher due to a smaller nearest neighbor distance when dispersion is included. Thus, the destabilizing effect from the electronic structure is added to the stabilization due to dispersion, generating an overall destabilization of the bcc phase for lithium with respect to fcc, contrary to all the other alkali metals. As shown in Figure 4, the Group 11 metals behave in the same way as lithium in this aspect. Because of the small energy differences involved leading to quasi-degenerate phases at 0 K, the dispersion correction plays a decisive role when determining the correct ground state structure of the bulk.

We notice that the PBE-D3 functional often overestimates the cohesive energy compared to the experimental values (Table 1), but this error should be mostly compensated by taking the energy difference for the cuboidal structures with respect to fcc along the Bain path. In this

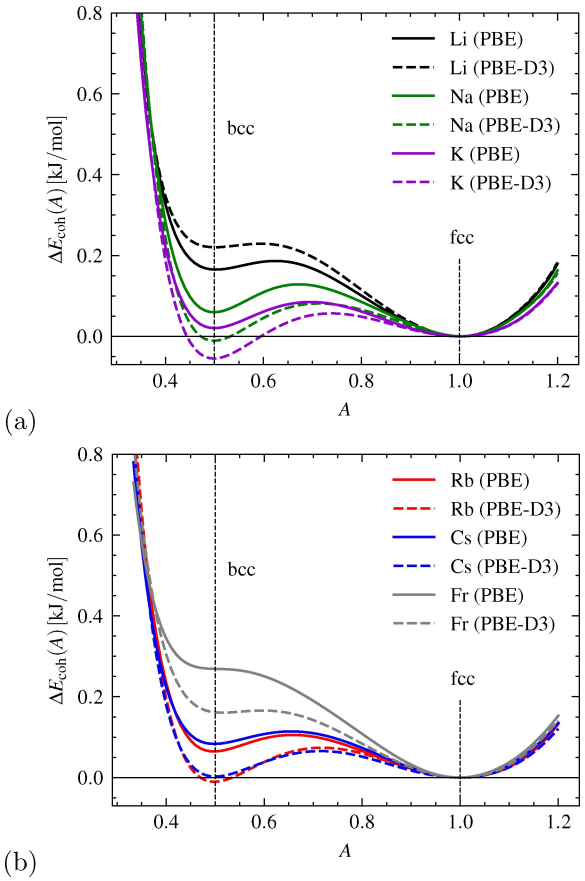

Figure 2. Cohesive energy of (a) lithium, sodium and potassium and (b) rubidium, cesium and francium relative to the fcc phase along the Bain path with the PBE functional and including dispersion interactions.

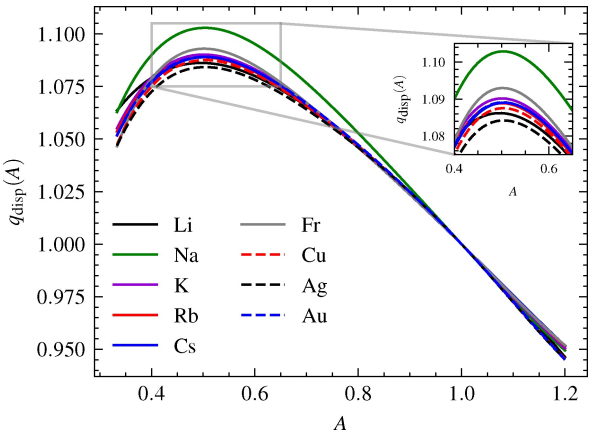

Figure 3. Ratio of dispersion energies along the cuboidal distortion path at the optimized PBE-D3 geometry for the Groups 1 and 11 metals. The inlet shows more details of the curves around the maximum.

Table 1: Optimized nearest neighbor distance R in Å, cohesive energies E_{coh} and zero-point energies E_0 in kJ/mol, location of the transition state $A^{\ddagger}$ in the Bain path and corresponding nearest neighbor distance $R^{\ddagger}$ and barrier height $\Delta E^{\ddagger}$ relative to the fcc structure in kJ/mol for the Groups 1 and 11 metals. $\Delta E = E_{coh}^{fcc} - E_{coh}^{bcc}$ and $\Delta E^{\ddagger} = E_{coh}^{fcc} - E_{coh}(A^{\ddagger})$ in kJ/mol. Experimental values are taken from Kittel.[14] Zero-point energy values in square brackets from Eq. (1), and exp. values are estimated from the Debye temperatures.[14]

Metal		R^{fcc}	R^{bcc}	$R^{\ddagger}$	$A^{\ddagger}$	E_{coh}^{fcc}	E_{coh}^{bcc}	ΔE	$\Delta E^{\ddagger}$	E_0^{fcc}	E_0^{bcc}	$\Delta E + \Delta E_0$
Li	PBE	3.065	2.978	2.986	0.625	155.152	154.987	0.165	0.187	3.971	3.842	0.036
	PBE-D3	2.959	2.880	2.885	0.595	172.251	172.030	0.220	0.229			0.091
	Exp.		3.023				158.0				[3.22]	
Na	PBE	3.742	3.635	3.655	0.672	109.141	109.081	0.060	0.129	[1.617]	[1.565]	0.008
	PBE-D3	3.635	3.532	3.559	0.712	125.016	125.027	−0.011	0.081			−0.063
	Exp.		3.659				107.0				[1.48]	
K	PBE	4.711	4.576	4.607	0.696	83.673	83.653	0.020	0.085	[0.878]	[0.850]	−0.008
	PBE-D3	4.603	4.469	4.511	0.739	95.214	95.269	−0.055	0.057			−0.083
	Exp.		4.525				90.1				[0.85]	
Rb	PBE	5.056	4.908	4.932	0.658	74.482	74.417	0.065	0.106	[0.534]	[0.517]	0.048
	PBE-D3	4.947	4.804	4.844	0.718	84.531	84.542	−0.011	0.074			−0.028
	Exp.		4.837				82.2				[0.52]	
Cs	PBE	5.502	5.336	5.360	0.655	68.642	68.559	0.083	0.114	[0.377]	[0.366]	0.072
	PBE-D3	5.386	5.233	5.271	0.715	76.987	76.984	0.002	0.066			−0.009
	Exp.		5.235				77.6				[0.36]	
Fr	PBE	5.499	5.326	–	–	61.079	60.810	0.269	–	[0.292]	[0.283]	0.260
	PBE-D3	5.367	5.202	5.218	0.596	70.611	70.449	0.161	0.166			0.152
	Exp.											
Cu	PBE	2.570	2.502	2.502	0.502	336.257	332.865	3.392	3.392	2.877	2.781	3.296
	PBE-D3	2.523	2.456	2.456	0.499	393.195	389.521	3.674	3.674			3.578
	Exp.	2.56				336.0				[3.21]		
Ag	PBE	2.932	2.859	2.858	0.499	243.013	240.034	2.979	2.979	[1.812]	[1.747]	2.914
	NR-PBE	3.009	2.933	2.933	0.500	218.742	216.273	2.469	2.469			2.404
	PBE-D3	2.879	2.806	2.805	0.500	298.848	295.340	3.509	3.509			3.444
	Exp.	2.89				284.0				[2.11]		
Au	PBE	2.939	2.860	2.860	0.499	292.883	290.911	1.972	1.972	[1.336]	[1.292]	1.928
	NR-PBE	3.128	3.049	3.049	0.500	219.553	216.807	2.745	2.745			2.701
	PBE-D3	2.900	2.822	2.822	0.501	355.012	352.738	2.273	2.273			2.229
	Exp.	2.88				368.0				[1.53]		

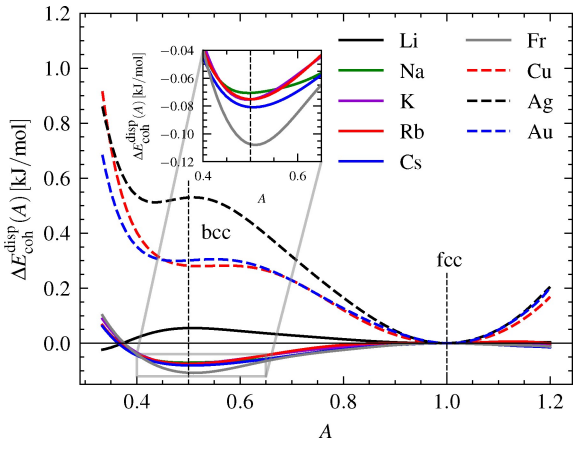

Figure 4. Change in the cohesive energy due to dispersion corrected geometries along the Bain path with respect to the fcc structure for the Groups 1 and 11 metals. The inlet shows more details of the curves around the minimum for the heavier Group 1 metals.

respect, Grimme's D4 dispersion correction[11] has been tested recently for the solid state with in general only slight improvements for lattice energies compared to the most widely used D3 approximation.[13]

For the Group 11 elemental solids we see a completely different picture, that is the bcc phase is not a local minimum anymore (see Figure 5), but rather a transition state towards a meta-stable minimum lying close to the so-called axial centered cuboidal lattice $A = 1/3$ with a coordination number of $N_{CN} = 10$.[15] The location of the transition state is practically unaltered by adding dispersion. In contrast, the location of the transition state (characterized by the distortion parameter $A^{\ddagger}$) along the Bain path for the alkali metals is close to the so-called self-dual mean-centered cubic lattice ($A = 1/\sqrt{2}$), which, in some sense, is an average between the bcc and fcc lattices as described in detail by Conway and Sloane.[15] This is even more apparent when dispersion is added, except for the lightest and heaviest Group 1 elements lithium and francium. The energy barrier to go from fcc to bcc ($\Delta E^{\ddagger}$) is however very small for

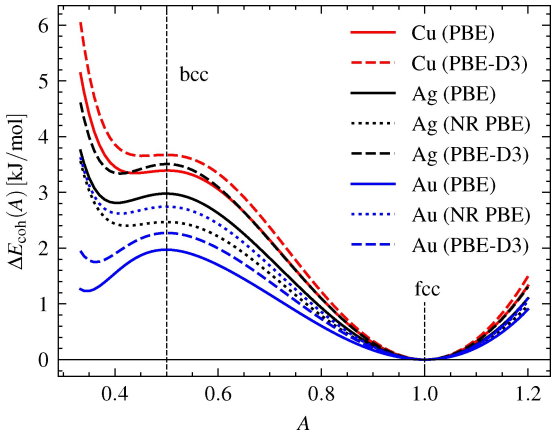

Figure 5. Cohesive energy of coinage metals relative to the fcc phase along the cuboidal transition path with the PBE functional including non-relativistic results for silver and gold.

the Group 1 elements and around 0.1 kJ/mol, with a decreasing tendency going down the group for the PBE functional, but less pronounced when dispersion interactions are included because of the change in the nearest neighbor distance and the corresponding electronic energy. The energy barriers for the coinage metals are considerably larger compared to the alkali metals. This implies that the bonding within the Group 11 atoms in the bulk is far stronger for the fcc phase with the highest coordination number compared to all the other cuboidal phases along the Bain distortion path as is evident from the cohesive energies listed in Table 1.

It was shown by Jerabek et al.[5] that the vibrational contributions to the free energy are of huge importance in stabilizing the bcc phase for lithium. As phonon calculations require a computationally expensive supercell treatment for sampling the *k*-space, and are often difficult to converge to the required accuracy, we used a simple model to calculate the zero-point vibrational energy (ZPE, E_0) within the harmonic approximation applying Badger's rule[16] for the heavier elements, and using lithium and copper as a reference system for the remaining Groups 1 and 11 elements, respectively. Within this model, the ratio between the ZPE of the reference element RE = Li or Cu to a heavier atom X is given by:

$$\frac{E_0^{X}(A)}{E_0^{RE}(A)} \approx \sqrt{\frac{R_{RE}^3(A) M_{RE}}{R_X^3(A) M_X}}, \qquad (1)$$

where E_0^X, R_X, and M_X are the zero-point energy, optimized nearest-neighbor distance and atomic mass of element X. $E_0^{RE}(A)$ is determined from elaborate phonon calculations (see computational details). Preliminary phonon dispersion calculations for Na show that this is an excellent approximation, and the trends with increasing mass are in line with Borelius.[17] Further, one can estimate the zero-point vibrational energy contributions from the Debye temperatures θ_D, i.e. $E_0 = \frac{9}{8} k_B \theta_D$, which are also listed in Table 1. These show that our simple model gives very accurate results for the zero-point vibrational contribution. We note that Li cannot be used as a reference for the Group 11 metals as the phonon dispersion curves between the Groups 1 and 11 elements are very different, and one cannot simply neglect the distance-dependent term in Eq. (1) as it leads to large errors otherwise. Adding the difference between the bcc and fcc ZPEs, ΔE_0, to the electronic contribution, we see from Table 1 that Li, Fr and all Group 11 elements prefer the fcc structure at 0 K, whilst the elements from Na to Cs prefer bcc. This is consistent with experiment[14] except for francium where no solid state data are available.

Concerning relativistic effects, which are enhanced for the Groups 11 and 12 elements,[18,19] for both silver and gold the nearest neighbor distances are shortened and the cohesive energies are increased substantially in agreement with previous work,[20] cf. Table 1. This produces an interesting behavior along the Bain path with the bcc phase being stabilized in gold but slightly destabilized in silver due to relativistic effects, see Figure 6. The relativistic stabilization in gold is however not enough to stabilize the bcc over the fcc phase. Furthermore, the meta-stable minimum located between acc and bcc is roughly at the same position as for the non-relativistic Bain path. In both cases, the relativistic effects in the differences in nearest neighbor distances and cohesive energies between fcc and bcc are very similar, see Table 1. Spin-orbit coupling, not considered here, might further influence these small energy differences.

In conclusion, the small energy differences between bcc and fcc for Group 1 metals makes dispersion and phonon contributions important for the question of which is the most stable phase at 0 K. For the Group 11 metals, fcc seems to be far more stabilized compared to bcc and both dispersion and phonon contributions do not change this trend. The activation barriers along the Bain bath from bcc to fcc are very small and comparable to a Lennard–Jones system,[21] and rearrangements can easily happen at more elevated temperatures. It was already pointed out that simple two-body interactions such as Lennard–Jones favour

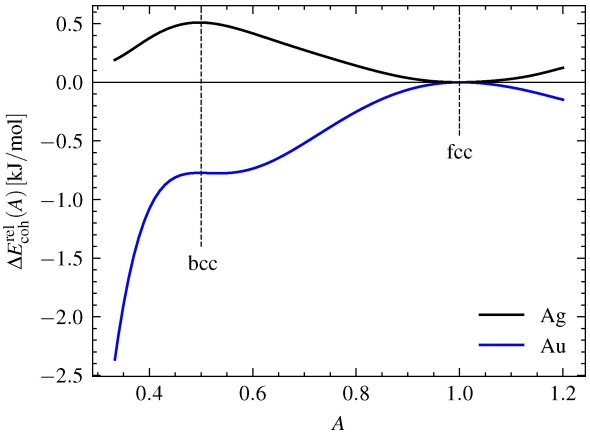

Figure 6. Change in the cohesive energy due to scalar relativistic corrections to the geometies along the Bain path with respect to the fcc structure for silver and gold.

the fcc phase,[21,22] and stabilizing the bcc phase at low temperatures requires higher than 2-body interactions. A simple harmonic oscillator model can be used to estimate the zero-point vibrational energy for the heavier elements using the lightest element in the same group as a reference system. Further investigations are underway to simulate the bcc to fcc phase transition for the Groups 1 and 11 metals at higher temperatures and pressures.

Computational Details

The bcc and fcc lattices are closely related as they are dual to each other. Following the ideas of Conway and Sloane,[15] it is therefore possible to build a connection between the two lattices through a smooth diffusionless (martensitic) transformation by defining a set of basis vectors **b** depending only on two lattice parameters, A and R, the first being responsible for the phase transition and the latter the nearest neighbor distance:

$$\mathbf{b}_1 = \frac{R}{\sqrt{A+1}}\begin{pmatrix}0\\1\\1\end{pmatrix}$$
$$\mathbf{b}_2 = \frac{R}{\sqrt{A+1}}\begin{pmatrix}\sqrt{A}\\0\\1\end{pmatrix} \quad (2)$$
$$\mathbf{b}_3 = \frac{R}{\sqrt{A+1}}\begin{pmatrix}\sqrt{A}\\1\\0\end{pmatrix}$$

with $R = \frac{a}{2}\sqrt{2+\left(\frac{c}{a}\right)^2}$ and $A = \frac{1}{2}\left(\frac{c}{a}\right)^2$. Here a and c are the lattice parameter of the basic bct (body-centered tetragonal) lattice as shown in Figure 1. The phase transition parameter A is characteristic of the Bain diffusionless martensitic transformation, which includes four important lattices along the path: the axial centered cuboidal lattice (acc, $A=1/3$), the bcc lattice ($A=1/2$), the mean centered cuboidal lattice (mcc, $A=1/\sqrt{2}$), and the fcc lattice ($A=1$). The volume of the lattice is related to the R and A parameters by:

$$V(R,A) = \frac{a^2 c}{2} = 2R^3\sqrt{\frac{A}{(A+1)^3}} \quad (3)$$

The bcc lattice has the largest volume within the Bain transformation path and hence the least dense packing density:

$$\rho(A) = \frac{\pi}{12}\sqrt{\frac{(A+1)^3}{A}} \quad (4)$$

Note that A classifies the crystal type, whereas the nearestneighbor distance just expands or contracts the volume.

For each value of A within the chosen interval of $[\frac{1}{3}, 1.2]$ in steps of 0.01, an optimization of the nearest-neighbor distance was performed for all systems using the Perdew–Burke–Ernzerhof (PBE) exchange-correlation functional[23] including dispersion corrections with the DFT-D3 approach and the Becke–Johnson damping.[24,25] The importance of dispersion forces for metallic systems is now well documented.[26] Additionally, non-relativistic calculations were carried out for both silver and gold.[27] All electronic structure calculations were performed with the VASP 6.4.0 version[28–31] with the atomic cores as described by Blöchl's Projector Augmented Wave (PAW) method[32,33] and the recommended pseudopotentials. The electronic optimization was done using the tetrahedron smearing method with Blöchl corrections[34] with an energy width of 0.1 eV. Convergence tests regarding k-spacing and energy cut-off were performed guaranteeing a variation of less than 1 meV in the total energy with respect to more demanding accuracy settings. The energy cut-off was set to 500 eV for Li, Na, Fr, Ag, and Au, 600 eV for Cu, 700 eV for Cs and 800 eV for K and Rb, respectively. The k-point grid was set using KSPACING = 0.07 and centered at the Γ point. To calculate the cohesive energy for each metal, the isolated atoms were placed in a slightly orthorhombic unit cell of size 14×14.001×14.002 Å^3 and their total energy was computed at the Γ point in reciprocal space. After minimization of the total electronic energy with respect to the nearest-neighbor distance, the variation of A for a given element creates a continuous reaction path $E_{coh}(A)$ along the specified lattices (Bain path).[9]

Phonon calculations on lithium and copper were performed using density functional perturbation theory with the aid of VASP 6.4.0 and Phonopy 2.14.0.[35] For this purpose, a 6×6×6 supercell was built with the optimized nearest-neighbor distance and the force constants were calculated with a Γ-centered 3×3×3 k-point grid for lithium and 4×4×4 k-point grid for copper.

Acknowledgements

We are grateful to the Alexander von Humboldt Foundation for financial support. Open Access publishing facilitated by Massey University, as part of the Wiley - Massey University agreement via the Council of Australian University Librarians.

Conflict of Interest

There are no conflicts of interest.

Data Availability Statement

Data sharing is not applicable to this article as no new data were created or analyzed in this study.

Keywords: Cohesive energies · Cuboidal phase transitions · Dispersion corrections · Groups 1 and 11 elements · Relativistic effects

[1] G. Frenking, S. Shaik, *The chemical bond: fundamental aspects of chemical bonding*, vol. 1, John Wiley & Sons **2014**.
[2] G. Frenking, S. Shaik, *The Chemical Bond: Chemical Bonding Across the Periodic Table*, vol. 2, John Wiley & Sons **2014**.

[3] V. V. Gusev, D. Adamson, A. Deligkas, D. Antypov, C. M. Collins, P. Krysta, I. Potapov, G. R. Darling, M. S. Dyer, P. Spirakis, M. J. Rosseinsky, *Nature* **2023**, *619*, 68.
[4] J. Maddox, *Nature* **1988**, *335*, 201.
[5] P. Jerabek, A. Burrows, P. Schwerdtfeger, *Chem. Commun.* **2022**, *58*, 13369.
[6] S. Alexander, J. McTague, *Phys. Rev. Lett.* **1978**, *41*, 702.
[7] N. Tugluoglu, R. H. Mutlu, *Phys. Rev. B* **1996**, *54*, 10253.
[8] W. Li, T. Wang, *Phys. Rev. B* **1999**, *60*, 11954.
[9] E. C. Bain, *Ind. Eng. Chem.* **1924**, *16*, 692.
[10] A. M. Teale, T. Helgaker, A. Savin, C. Adamo, B. Aradi, A. V. Arbuznikov, P. W. Ayers, E. J. Baerends, V. Barone, P. Calaminici, E. Cancès, E. A. Carter, P. K. Chattaraj, H. Chermette, I. Ciofini, T. D. Crawford, F. De Proft, J. F. Dobson, C. Draxl, T. Frauenheim, E. Fromager, P. Fuentealba, L. Gagliardi, G. Galli, J. Gao, P. Geerlings, N. Gidopoulos, P. M. W. Gill, P. Gori-Giorgi, A. Görling, T. Gould, S. Grimme, O. Gritsenko, H. J. A. Jensen, E. R. Johnson, R. O. Jones, M. Kaupp, A. M. Köster, L. Kronik, A. I. Krylov, S. Kvaal, A. Laestadius, M. Levy, M. Lewin, S. Liu, P.-F. Loos, N. T. Maitra, F. Neese, J. P. Perdew, K. Pernal, P. Pernot, P. Piecuch, E. Rebolini, L. Reining, P. Romaniello, A. Ruzsinszky, D. R. Salahub, M. Scheffler, P. Schwerdtfeger, V. N. Staroverov, J. Sun, E. Tellgren, D. J. Tozer, S. B. Trickey, C. A. Ullrich, A. Vela, G. Vignale, T. A. Wesolowski, X. Xu, W. Yang, *Phys. Chem. Chem. Phys.* **2022**, *24*, 28700.
[11] E. Caldeweyher, C. Bannwarth, S. Grimme, *J. Chem. Phys.* **2017**, *147*, 034112.
[12] I. S. Lim, M. Pernpointner, M. Seth, J. K. Laerdahl, P. Schwerdtfeger, P. Neograd, M. Urban, *Phys. Rev. A* **1999**, *60*, 2822.
[13] E. Caldeweyher, J.-M. Mewes, S. Ehlert, S. Grimme, *Phys. Chem. Chem. Phys.* **2020**, *22*, 8499.
[14] C. Kittel, *Introduction to Solid State Physics*, John Wiley & Sons, Inc., New York **2004**.
[15] J. H. Conway, N. J. A. Sloane, *J. Number Theory* **1994**, *48*, 373.
[16] R. M. Badger, *J. Chem. Phys.* **1934**, *2*, 128.
[17] G. Borelius, *Phys. Scr.* **1978**, *18*, 9.
[18] P. Pyykkö, *Chem. Rev.* **1988**, *88*, 563.
[19] P. Schwerdtfeger, O. R. Smits, P. Pyykkö, *Nat. Chem. Rev.* **2020**, *4*, 359.
[20] N. Takeuchi, C. T. Chan, K. M. Ho, *Phys. Rev. B* **1989**, *40*, 1565.
[21] A. Burrows, S. Cooper, P. Schwerdtfeger, *Phys. Rev. E* **2021**, *104*, 035306.
[22] P. Schwerdtfeger, A. Burrows, O. R. Smits, *J. Phys. Chem. A* **2021**, *125*, 3037.
[23] J. P. Perdew, K. Burke, M. Ernzerhof, *Phys. Rev. Lett.* **1996**, *77*, 3865.
[24] S. Grimme, J. Antony, S. Ehrlich, H. Krieg, *J. Chem. Phys.* **2010**, *132*, 154104.
[25] S. Grimme, S. Ehrlich, L. Goerigk, *J. Comput. Chem.* **2011**, *32*, 1456.
[26] A. A. Adeleke, E. R. Johnson, *Phys. Rev. B* **2023**, *107*, 064101.
[27] S. Löffelsender, P. Schwerdtfeger, S. Grimme, J.-M. Mewes, *J. Am. Chem. Soc.* **2021**, *144*, 485.
[28] G. Kresse, J. Hafner, *Phys. Rev. B* **1993**, *47*, 558.
[29] G. Kresse, J. Hafner, *Phys. Rev. B* **1994**, *49*, 14251.
[30] G. Kresse, J. Furthmüller, *Comput. Mater. Sci.* **1996**, *6*, 15.
[31] G. Kresse, J. Furthmüller, *Phys. Rev. B* **1996**, *54*, 11169.
[32] P. E. Blöchl, *Phys. Rev. B* **1994**, *50*, 17953.
[33] G. Kresse, D. Joubert, *Phys. Rev. B* **1999**, *59*, 1758.
[34] P. E. Blöchl, O. Jepsen, O. K. Andersen, *Phys. Rev. B* **1994**, *49*, 16223.
[35] A. Togo, I. Tanaka, *Scr. Mater.* **2015**, *108*, 1.

Manuscript received: September 14, 2023
Accepted manuscript online: October 25, 2023
Version of record online: November 29, 2023